


Systematic study of Coulomb confinement resonances of atoms trapped inside charged fullerenes

Afsal Thuppilakkadan,¹ Jobin Jose,² and Hari R. Varma¹¹*School of Basic Sciences, IIT Mandi, Mandi-175005, Himachal Pradesh, India*²*Department of Physics, IIT Patna, Bihta-801103, Bihar, India* (Received 6 July 2020; revised 16 October 2020; accepted 2 December 2020; published 30 December 2020)

An earlier work of Dolmatov *et al.* [*Phys. Rev. A* **73**, 013201 (2006)] on Ne inside a charged fullerene ($\text{Ne}@C_{60}^{q=-3,-5}$) has revealed the presence of two unusually large confinement resonances termed Coulomb confinement resonances (CCRs); the first CCR is narrow and the second one is broad and their origins are attributed to the presence of charge on the fullerene surface. The present work extends this study to other subshells and also to other systems such as $\text{Ar}@C_{60}^q$ and $\text{Xe}@C_{60}^q$ using relativistic random phase approximation, but with an aim to investigate the genesis of the CCRs. Further, a detailed analysis of these resonances within a single active electron approximation unearths an interesting difference associated with the origin of these two CCRs. The photoionized electron is temporally trapped in the C_{60} confinement well for the case of narrow resonance and in the atomic well region for the case of broad resonance. Also, the present work shows that the broad resonance can occur even for the case of $q = 0$ and is demonstrated for $\text{Xe}@C_{60}^q$ as a test case.

DOI: [10.1103/PhysRevA.102.062826](https://doi.org/10.1103/PhysRevA.102.062826)

I. INTRODUCTION

The spectroscopic information of endohedral systems such as an atom encapsulated inside fullerene C_{60} ($A@C_{60}$, $A = \text{atom}$) contributes very useful data to our fundamental understanding and also to practical applications. From a fundamental point of view, such confined atomic systems provide deeper insights into the nature of electron correlations and relativistic interactions and offer new avenues to test various many-body theories. On the practical fronts, they hold the prospect of exciting applications in quantum computing [1], superconductivity of materials [2], biomedical fields [3], photovoltaic devices [4], etc. Organometallic molecules based on C_{60} are proposed as hydrogen (H) storage materials for fuel cells in electric vehicles [5]. The presence of endohedral systems with noble atoms inside in extraterrestrial environments points out their relevance in astrophysics [6].

Many intriguing phenomena are associated with the photoionization of confined atomic systems. To date, a myriad of theoretical works unraveling different aspects of photoionization of endohedral fullerenes have been reported [7–20]. The photoionization spectrum of atom inside fullerene is dominated by the ubiquitous confinement oscillations which induce dramatic differences to the ionization spectra compared to the corresponding spectra from the free atom. These confinement oscillations encode geometrical information about the endohedral environment [21]. They are very sensitive to the correlations and relativistic effects in the atom. The presence of confinement oscillations engenders spin-orbit interaction activated interchannel coupling (SOIAC) structures and makes its appearance a regular feature in confined systems more than in free atoms [22–24]. Photoionization studies of these resonances, therefore, provide important impetus to our fundamental understanding and enable different ways to control the light-matter interactions. Note that the confinement

oscillations aka confinement resonances are present in $e-A@C_{60}$ scattering processes [25,26] as well. A series of experiments were also done at Berkeley advanced light source using merged beam techniques [27–29]. Since the experimental studies on endohedral systems are in a nascent stage, it is important to investigate different features of the photoionization spectrum through theoretical studies. These explorations will enable us to distinguish features of the photoionization spectrum that originate from the atom or fullerene and that result from the interference of atomic and fullerene electrons.

There are, in general, three kinds of confinement resonances seen in the photoionization dynamics of such systems: (i) ordinary confinement resonances (OCRs) [16] which are due to the interference of the outgoing photoelectron wave with the scattered photoelectron from the confining well; (ii) Coulomb confinement resonances (CCRs) [30,31] that arise because of the interference between the outgoing photoelectron wave with that of the reflected waves from the Coulomb barrier and from the C_{60} shell; (iii) resurrected confinement resonances [13,32] due to interchannel coupling.

The present work is essentially motivated by the earlier work of Dolmatov *et al.* [30], who reported the presence of CCR in the $1s$ subshell of $\text{Ne}@C_{60}^q$, where “ q ” refers to the charged state of the fullerene. The presence of a charged fullerene induces CCRs and these resonances dominate the $1s$ cross section. For $q = -3$ and $q = -5$, two CCRs have been reported in which the first resonance is very narrow and the second one is relatively broad. A subsequent work [32] showed the revivification of confinement resonances in the $2p$ subshell of $\text{Ne}@C_{60}^{q=-5}$ at very high energies due to the presence of $1s$ CCR. Wigner time delay studies on $\text{Ne}@C_{60}^{q=-5}$ have also been reported [13]. The objective of the present work is twofold: first to see if the CCRs are present in other subshells and also in other confined atomic systems and further to check if they are peculiar to the confinement by C_{60}

anions alone, and second, to draw the similarities and differences in the two CCRs in terms of their nature and origin, which are yet to be understood in detail.

In order to accomplish the aforementioned objectives, photoionization studies of innermost and penultimate subshells of Ne@C₆₀^q, Ar@C₆₀^q, and Xe@C₆₀^q have been carried out using the relativistic random phase approximation (RRPA). We show that CCR is not just a feature of the 1s cross section but also appears in the 2s subshell. In addition, the presence of CCR is also shown for other systems such as Ar@C₆₀^{q=-4} and Xe@C₆₀^{q=-3}. Moreover, detailed studies have been undertaken about the origin of these resonances within single active electron (SAE) approximation using the model potential employed in Ref. [33], hereafter referred to as the Tong-Lin potential. Using the probability density of the continuum wave and the potential seen by the photoelectron, we find that the origin of the two resonances differs from each other with regard to the region of resonant trapping. Using the results of Xe@C₆₀^{q=0}, it is also shown that the charge on the fullerene is not imperative for the appearance of the broad resonance.

A brief discussion of the theoretical methodologies used in the present work is given in Sec. II. Results and discussions are provided in Sec. III. Finally, in Sec. IV, the summary and conclusions are provided.

II. METHODOLOGY

The endohedral environment is simulated by adopting the same model used in the work of Dolmatov *et al.* [30]. The atom is placed at the center of the neutral fullerene cage, which is modeled by a spherically attractive potential (V^{cage}) with inner radius $R_{\text{in}} = 5.8$ a.u. and thickness $\Delta = 1.9$ a.u. and is given by

$$V^{\text{cage}}(r) = \begin{cases} -U_0, & \text{if } R_{\text{in}} \leq r \leq R_{\text{in}} + \Delta \\ 0, & \text{otherwise.} \end{cases} \quad (1)$$

Here $U_0 = 0.3021$ a.u. which is obtained by fitting with the experimental data on the size and electron affinity (2.65 eV) for C₆₀. This model has been successfully applied in a number of theoretical works to bring out some of the key features resulting from confinement [7,9,17,34]. Furthermore, for accounting the additional charge, it is assumed that the excess charge is evenly distributed over the cage surface. It results in the emergence of additional Coulomb forces which can be easily obtained by using Gauss' law and is given by the following:

$$V^q(r) = \begin{cases} \frac{q}{R_{\text{in}} + \Delta} & \text{if } 0 < r < R_{\text{in}} + \Delta \\ \frac{q}{r} & \text{otherwise.} \end{cases} \quad (2)$$

The effective confinement potential is accordingly defined as $V_{\text{cq}}(r) = V^{\text{cage}}(r) + V^q(r)$. This potential is added to the atomic potential to calculate the ground state and continuum photoelectron wave functions and ground state energies of the encapsulated atom.

In this work the photoionization cross section is calculated in two different ways: first by using relativistic random phase approximation (RRPA) and second by using single active electron approximation (SAE) with the Tong-Lin potential.

TABLE I. Tong-Lin parameters for Ne, Ar, and Xe [33,41].

Atom	a_1	a_2	a_3	a_4	a_5	a_6
Ne	8.069	2.148	-3.570	1.986	0.931	0.602
Ar	16.039	2.007	-25.543	4.525	0.961	0.443
Xe	51.356	2.112	-99.927	3.737	1.644	0.431

The initial state of the atom in RRPA is constructed using the Dirac-Hartree-Fock (DHF) methodology. A detailed description of the RRPA methodology can be found elsewhere [35–37]. It is to be noted that the RRPA can be very effectively used to study the role of correlation in the form of interchannel coupling by performing calculations at various levels of coupling of the ionization channels. For Ne@C₆₀^q and Ar@C₆₀^q, calculations are performed at two different levels by involving (i) only the two ionization channels (2 ch) from the ns subshell ($n = 1$ or 2), (ii) all the subshells which correspond to the coupling of nine ionization channels (9 ch) for Ne@C₆₀^q and sixteen ionization channels (16 ch) for Ar@C₆₀^q. For the case of Xe@C₆₀^q the calculations are carried out by coupling the ionization channels from s subshell only (2 ch).

The primary reason behind the appearance of CCRs is the presence of the endohedral environment surrounding the system. A detailed analysis regarding its origin is possible by carrying out the photoionization calculations in SAE approximation, by which the effect of confinement can be isolated from correlations. This is to minimize interference effects of correlation and CCRs so that the genesis of the latter is unambiguously identified. The origin of CCRs has been scrutinized looking at the resonant Coulomb wave function, which is obtained rather easily in the SAE approach. Here, the Tong-Lin potential is used to model the screening effects of residual electrons. This method has been employed successfully in the past in a number of important atomic physics problems [10,38–40]. In this model [33] the screening effects due to the residual interaction is simulated by

$$V_{\text{T}}(r) = -\frac{Z_c + a_1 e^{-a_2 r} + a_3 r e^{-a_4 r} + a_5 e^{-a_6 r}}{r}. \quad (3)$$

Here $Z_c = 1$ is the charge seen by the electron asymptotically. The values of the various parameters (a_1 to a_6) for Ne, Ar, and Xe are obtained from literature and are listed in Table I [33,41].

The radial wave function of ground and continuum states are calculated by solving the Schrodinger equation in spherical symmetric coordinates,

$$\frac{d}{dr} \left[r^2 \frac{dR(r)}{dr} \right] = 2r^2 [V_{\text{eff}} - E]R(r), \quad (4)$$

where $V_{\text{eff}} = \frac{\ell(\ell+1)}{2r^2} + V_{\text{T}}(r) + V_{\text{cq}}(r)$.

The ground state energies obtained by using the Dirac-Hartree-Fock method (DHF) and SAE approximation are given in Table II. For comparison, experimental binding energies of the free atomic systems are also provided. The energy values predicted by the SAE formalism finds fairly good agreement with the DHF and experimental thresholds. This agreement encourages us to use the Tong-Lin model potential

TABLE II. Binding energies obtained using DHF and SAE approximations along with the available experimental values.

Systems	1s threshold (a.u.)			2s threshold (a.u.)		
	DHF	SAE	Experiment	DHF	SAE	Experiment
Free Ne	32.817	31.904	31.979 [42]	1.935	1.627	1.779 [42]
Ne@C ₆₀ ^{q=0}	32.817	31.904		1.935	1.627	
Ne@C ₆₀ ^{q=-5}	32.168	31.252		1.286	0.977	
Free Ar	119.126	113.769	117.816 [42]	12.411	11.018	11.991 [42]
Ar@C ₆₀ ^{q=0}	119.129	113.769		12.414	11.018	
Ar@C ₆₀ ^{q=-4}	118.609	113.246		11.895	10.498	
Free Xe	1277.226	1235.588	1270.126 [43]	202.461	197.950	200.389 [43]
Xe@C ₆₀ ^{q=0}	1277.247	1235.588		202.481	197.950	
Xe@C ₆₀ ^{q=-3}	1276.858	1235.032		202.092	197.565	

for further photoionization studies, in particular, to delineate the effects of correlation and confinement effects.

The photoionization cross section is then obtained by using the formula [44]

$$\sigma = \frac{4\pi^2}{3} \alpha N_{nl} E_{ph} |\langle R_{\epsilon l} | r | R_{nl} \rangle|^2. \quad (5)$$

Here $\alpha = 1/137$ a.u. is the fine structure constant, N_{nl} is the number of electrons in the nl subshell, and E_{ph} is the incident photon energy. $R_{\epsilon l}$ and R_{nl} are the continuum and ground state wave functions respectively, obtained by solving Eq. (4) for the corresponding energies.

III. RESULTS AND DISCUSSION

Figures 1 and 2 show respectively the $1s$ and $2s$ dipole cross sections of Ne@C₆₀^{q=0} and Ne@C₆₀^{q=-5} along with the free Ne calculated using the RRPA in two different levels of truncations as mentioned in Sec. II. For Ne@C₆₀^{q=0,-5}, 2 ch and 9 ch results of the $1s$ cross section are nearly the same (Fig. 1) because $1s$ is far away from the thresholds of $2s$ and

$2p$ subshells. The free Ne cross section decreases monotonically from the threshold, while the encapsulated Ne cross section for both $q = 0$ and $q = -5$ exhibit confinement oscillations above their respective thresholds. Notice that above the $1s$ threshold for the case $q = 0$, the confinement oscillations, for Ne@C₆₀^{q=0,-5}, overlap each other and these resonances are the OCRs. The dominant feature of the cross section profile is the two resonances appearing just above the Ne@C₆₀^{q=-5} threshold at 32.556 and 32.758 a.u. photon energies. These additional resonances seen in Ne@C₆₀^{q=-5} cross section as compared to Ne@C₆₀^{q=0} are the CCRs. The presence of CCR in $1s$ and its impact on other subshells via interchannel coupling have been reported earlier [13,32].

The present work shows that the CCR is not just a feature in $1s$ but it is also present in other subshells. It is to be noted that the $1s$ and $2s$ cross section profiles differ for the case of free Ne. The $1s$ cross section decreases monotonically from the threshold while the $2s$ cross section (Fig. 2) increases from the threshold. This is because of the presence of a Cooper minimum in the discrete region of $2s$ [45].

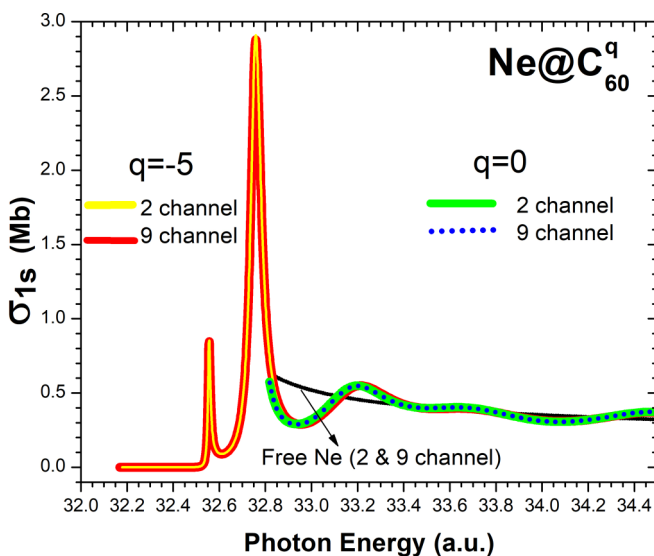


FIG. 1. RRPA photoionization cross section of $1s$ subshell of Ne@C₆₀^q ($q = 0$ and $q = -5$) in two levels of truncation along with free Ne cross section.

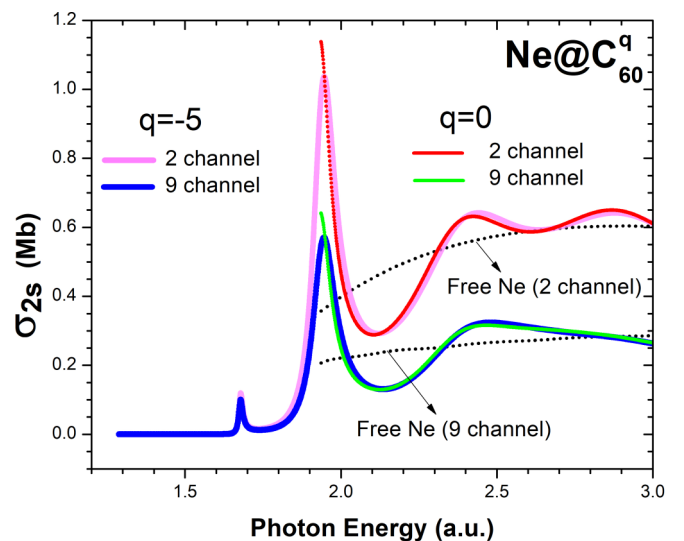


FIG. 2. RRPA photoionization cross section of $2s$ subshell of Ne@C₆₀^q ($q = 0$ and $q = -5$) in two levels of truncation along with free Ne cross section.

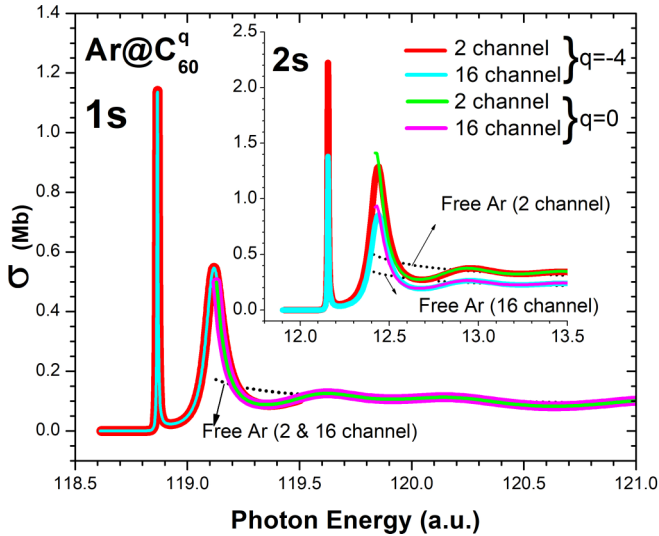


FIG. 3. RRP photoionization cross section of $1s$ and $2s$ subshell of $\text{Ar}@C_{60}^q$ ($q = 0$ and $q = -4$) in two levels of truncation along with free Ar cross section.

The confinement enhances the $2s$ cross section of $\text{Ne}@C_{60}^{q=0}$ as compared to free Ne case at its threshold. The enhancement is less for $q = -5$ in comparison with $q = 0$ at the threshold of $\text{Ne}@C_{60}^{q=0}$. This behavior is just in contrast with that in the case of the $1s$ cross section of $\text{Ne}@C_{60}^{q=0, -5}$; the $1s$ cross sections of $q = 0$ and $q = -5$ are identical at the threshold of $\text{Ne}@C_{60}^{q=0}$ (Fig. 1). This change in the trends in $1s$ and $2s$ subshell cross sections to the charge distributions on the C_{60} cage is owing to the fact that the former subshell wave function is close to the nucleus of Ne, which does not “feel” the changes in the electron density on the cage. On the other hand, the $2s$ wave function is in the vicinity of the C_{60}^q confinement. These changes in the C_{60}^q interaction potential, therefore, are preferentially modifying the $2s$ relative to $1s$.

Similar to the case of $1s$, the $2s$ cross section of $\text{Ne}@C_{60}^{q=-5}$ also shows CCRs and OCRs. Unlike for the case of $1s$, the 2 ch and 9 ch results differ because the $2s$ subshell threshold is close to that of the $2p$ subshell; as a result the interchannel coupling with $2p$ significantly modifies the CCRs and OCRs of $2s$. Also, the magnitude of CCRs is relatively smaller in $2s$ as compared to $1s$. In the $1s$ cross section, the amplitude of CCRs is above the OCRs, while in the case of the $2s$ cross section, the amplitude of OCRs is higher compared to the first CCR. It is noteworthy that the $1s$ (Fig. 1) and $2s$ (Fig. 2) cross sections of $\text{Ne}@C_{60}^{q=0}$ at their corresponding thresholds are falling on the tail of the second CCR of $\text{Ne}@C_{60}^{q=-5}$ from their respective $1s$ and $2s$ cross sections. The analysis shows, although not conclusive but of course suggestive, that the CCR can be even formed in $A@C_{60}^{q=0}$.

As discussed in the work of Dolmatov and Manson [30], the origin of CCR is attributed to the presence of a charge induced Coulomb barrier, seen by the photoelectron. As there is nothing special about $\text{Ne}@C_{60}^q$, it is now interesting to look for other endohedral species in the same group. In Fig. 3, we show the results from $\text{Ar}@C_{60}^q$. The overall qualitative behavior is the same as that of $\text{Ne}@C_{60}^q$. The $1s$ cross section

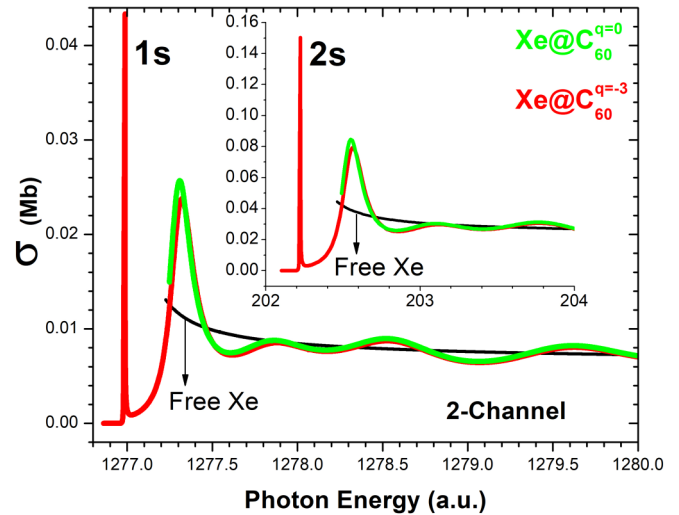


FIG. 4. RRP photoionization cross section of $1s$ and $2s$ subshell of $\text{Xe}@C_{60}^q$ ($q = 0$ and $q = -3$) along with free Xe cross section.

in $\text{Ar}@C_{60}^{q=0}$ shows only ordinary confinement resonances while $\text{Ar}@C_{60}^{q=-4}$ shows both OCR and CCR. The $2s$ cross section, shown in the inset, also displays a similar behavior but is sensitive to the electron correlation through the interchannel coupling. The tail part of the second CCR in the $q = -5$ cross section coincides with that in the case of $q = 0$ at the threshold.

The $1s$ and $2s$ cross sections of $\text{Xe}@C_{60}^q$ for $q = 0$ and -3 are shown in Fig. 4 along with the free Xe results. Here it is seen that both $1s$ and $2s$ profiles show the higher energy CCR even for the case of $q = 0$. However, the lower energy resonance appears only if the charge is present on fullerene. In other words, when the charge state of fullerene is increased from $q = 0$ to $q = -3$, a narrow resonance appears near the threshold. The broad resonance (second CCR) in the higher energy region, seen for the case of $\text{Xe}@C_{60}^{q=-3}$, is also present as the first resonance in the $q = 0$ case. This is indicative of an inherent difference in the origin of these two resonances. This prompted us to explore the origin of these two resonances in a detailed way. It is to be noted that different charged states were used in order to avoid some numerical convergence issues.

A qualitative description of the origin of CCRs in the $1s$ cross section for $\text{Ne}@C_{60}^q$ is provided in the work of Dolmatov and Manson [30]. However, the work does not, in detail, look for the differences in the features of the two resonances. For example, it is seen from Fig. 1 that the first resonance is relatively smaller and sharper compared to the second resonance. The contrasting differences in the two CCRs are explored in the present work using SAE approximation. The analysis is presented for the innermost subshells of the endohedral atoms we considered; the same analysis is applicable for the CCRs in the $2s$ subshells also.

The cross section is essentially proportional to the overlap integral of initial and final state wave functions. The initial state wave function of the innermost subshell electron is not at all affected by the external environment. The features in the cross section, therefore, are essentially dictated by the confinement induced modifications in the continuum state.

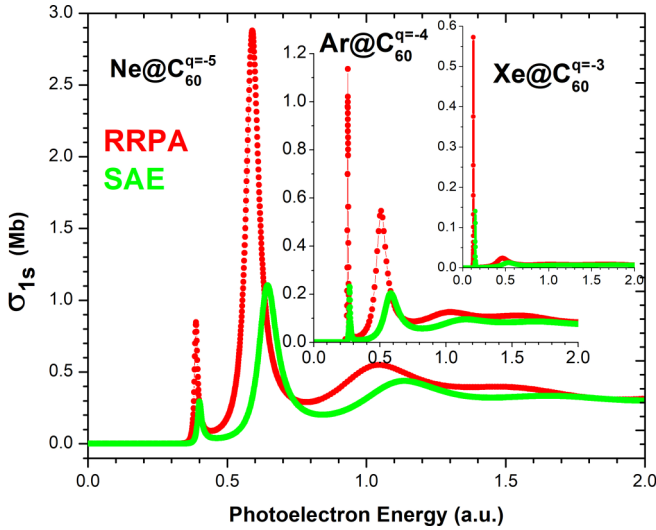


FIG. 5. RRPA (red curve) and SAE (green curve) photoionization cross section of $1s$ subshell of $\text{Ne}@C_{60}^{q=-5}$, $\text{Ar}@C_{60}^{q=-4}$, and $\text{Xe}@C_{60}^{q=-3}$.

In order to understand the impact of confinement it is better to separate out the correlation effects on the photoionization parameters. The required initial and final states, therefore, are generated within the SAE approximation.

In Fig. 5 is shown the $1s$ cross section obtained within SAE along with the RRPA results for all systems under consideration. As seen, SAE results qualitatively agree with the RRPA results reproducing the CCRs and OCRs although the actual magnitude and positions of these resonances somewhat differ. The quantitative difference is of course originating from the omission of the RRPA correlation in the rudimentary SAE approximation. To illustrate this further, one may write the continuum wave function in the RRPA as a perturbative series,

in which the first term is the uncorrelated IPA wave function and the other terms are higher-order corrections introduced due to the RRPA correlation effects [46,47]. It is to be noted that the IPA wave function in the perturbative expansion is similar to the continuum electron wave function in the SAE approach. Therefore, the quantitative differences are bound to be there between the SAE approximated and RRPA results. The qualitative agreement is also not surprising, as the $1s$ electron is dominated by the strong nuclear Coulomb field, in which the correlation effects are less dominant [48]. This qualitative agreement in the cross section allows us to study the origin of confinement resonances using the SAE approximation. Note that even the qualitative agreement can be at risk for higher subshell cases, where correlation effects are governing the dynamics.

We aim to investigate the resonant wave function of the photoelectron at different energies, so that analysis of the nature of localized electron across the resonant region is possible. Several energy points are selectively chosen to understand the evolution of the continuum states in response to the change in photoelectron energy across the region of this resonance. Figure 6(a) is the magnified version of first CCR of $\text{Ne}@C_{60}^{q=-5}$; the vertical lines labeled as L1 to L3 and R1 and R2 are respectively the energy points selected from the left and right sides of this resonance peak. The corresponding photoelectron energies are also listed in the figure. The label Res.1 corresponds to the energy at the first resonance. Figure 6(b) shows the evolution of ϵp photoelectron probability densities corresponding to various continuum states (L1 to L3, Res.1, and R1 and R2) along with the ground state probability density ($1s$).

Also shown in Fig. 6(b) is the potential seen by the ϵp photoelectron ejected from the $1s$ subshell. This potential is the sum of atomic potential and confining potential due to the charged fullerene. The potential curve is characterized by two wells. The first well is formed due to the combination of

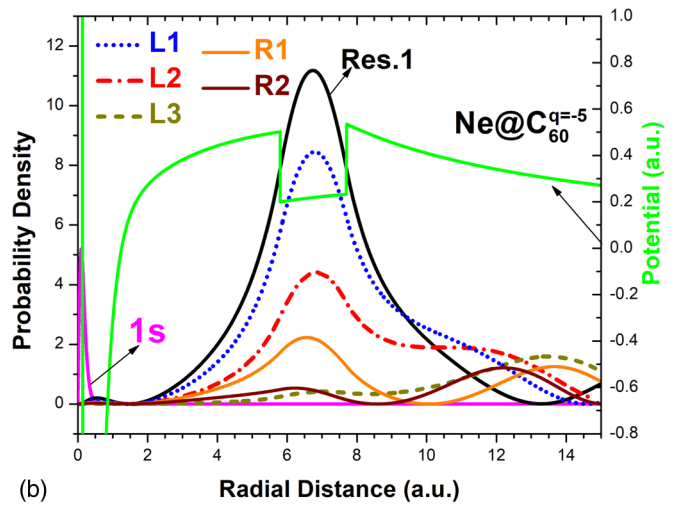
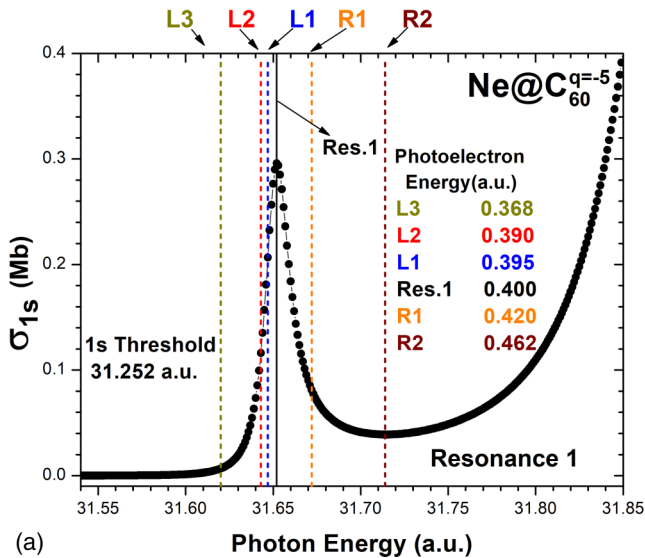


FIG. 6. (a) First resonance of the photoionization cross section of $1s$ subshell of $\text{Ne}@C_{60}^{q=-5}$. The vertical lines labeled L3 to L1 and R1 and R2 are the energy points on the left and right side of the resonant peak (Res.1). The photoelectron energy corresponding to the labels are listed in the figure. (b) Probability density corresponding to the labels in (a) along with the potential seen by the photoelectron ϵp . Ground state wave function is also plotted.

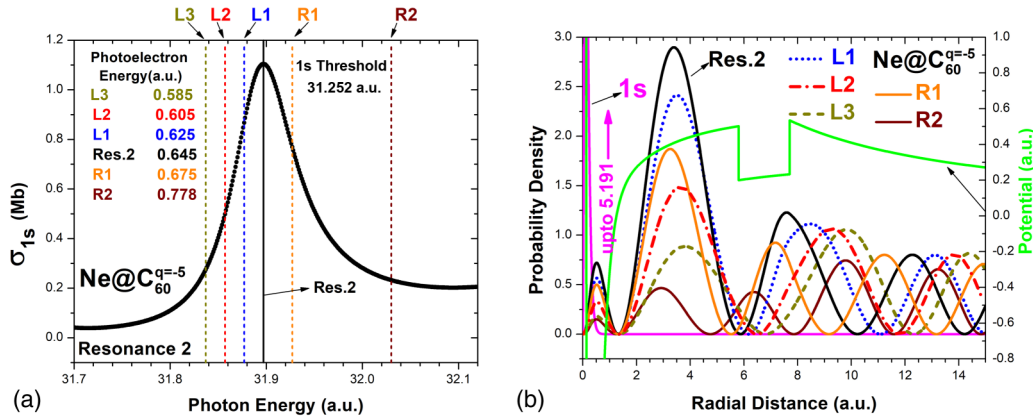


FIG. 7. (a) Second resonance of the photoionization cross section of $1s$ subshell of $\text{Ne}@C_{60}^{q=-5}$. The vertical lines labeled L3 to L1 and R1 and R2 are the energy points on the left and right side of the resonant peak (Res.2). The photoelectron energy corresponding to the labels are listed in the figure. (b) Probability density corresponding to the labels in (a) along with the potential seen by the photoelectron εp . Ground state wave function is also plotted.

the intrinsic electrostatic potentials of the atom (the Tong-Lin potential in this case) and the repulsive centrifugal barrier. The impact of the confining potential does not affect the shape of the first well since it is a constant in the specified region as shown in Eq. (2). A second well is seen between 5.8 and 7.7 a.u. owing to the fullerene potential as described in Eq. (1). From Fig. 6(b), it can be seen that the resonant trapping occurs in this second well which is evident from the significant localization of the final state (εp) electron there. As the photoelectron energy moves from L3 to L1, the localization of the probability density in this region increases and reaches a maximum for Res.1 which is the final state corresponding to the peak of the first resonance. After Res.1, the localization begins to decrease as the photoelectron energy increases further.

A similar analysis is carried out for the second resonance. Figure 7(a) is the magnified version of the second resonance of the cross section, the labels L1 to L3 and R1 and R2 are the energy points selected from the left and right sides of the resonance peak, respectively, and Res.2 is the maximum at the second resonance. Figure 7(b) shows the probability density of the ground state along with the various continuum states corresponding to the energy points mentioned in Fig. 7(a). The potential seen by the εp photoelectron ejected from the $1s$ subshell is also shown. Here again a localization happens for the final states, however, it occurs in the region before the confinement well. Similar to the case of first resonance, the localization is maximum at the resonance (labeled by Res.2) and decreases for energies lesser or greater than the resonant energy. The aforementioned analysis concludes that the first CCR (sharp) is due to a resonant trapping of the photoelectron in C_{60} well, whereas the second one (broad) is due to that in the atomic well *modified* in the presence of additional charges on the fullerene. Although both the resonances have a different origin, they are eligible to be called CCRs as the additional Coulomb potential supports the two.

Since the first resonance occurs in the confinement well, this can be more appropriately labeled as “well states.” These states are similar to the unbound C_{60} orbitals as discussed in the work of Ref. [49]. Although we use a simple model, this includes an average effect of interaction of fullerene electrons and protons. Therefore, the presence of the first resonance

cannot be obliterated even in a more sophisticated molecular level calculations although the quantitative details are likely to be changed. To check the viability of this assumption, we have now altered the parameters of confinement systematically. We have first performed RRPA calculations based on two other sets of parameters used for modeling fullerene: (i) $R_{in} = 6.01$ a.u., $\Delta = 1.25$ a.u., and $U_0 = 0.422$ a.u. [50]; (ii) $R_{in} = 5.262$ a.u., $\Delta = 2.91$ a.u., and $U_0 = 0.2599$ a.u. [49]. Earlier studies using set (i) shows better agreement with experimental results on photoionization [29] and set (ii) has been successfully employed in scattering studies of fullerene [49]. These are shown in Fig. 8(a) along with the original parameters employed in our calculations ($R_{in} = 5.8$ a.u., $\Delta = 1.9$ a.u., and $U_0 = 0.3021$ a.u.), denoted as set (iii) parameters. Despite the quantitative differences, one may notice that the CCRs are qualitatively alike in all model potential calculations. This suggests that the CCRs are sensitive to different model potentials, however, their presence is guaranteed in $A@C_{60}^{q<0}$ cases. However, it is not possible to do any systematic analysis using these sets of parameters because of the way they differ from each other. So, we have further carried out studies by using set (iii), but varying systematically one parameter at a time. Figures 8(b)–8(d) show these results by varying the radius, delta, and depth of the potential respectively while keeping the other parameters in set (iii) fixed. It is seen that CCRs are present in all these calculations irrespective of the values of the parameters employed although their quantitative details differ. The direct part of the DHF potentials experienced by the photoelectron for all cases are also shown as inset figures. Using these the sensitivity of resonance positions can be easily understood. The barrier height and the depth of the confining potential vary in all cases as shown in the insets of Figs. 8(a)–8(c) whereas in Fig. 8(d) only the depth (V^{cage}) varies.

It must be remembered that the barrier for the first (sharp) CCR is due to the C_{60} well and that for the second (broad) one is attributed to the atomic well. Hence, the alterations in the barrier shapes at these two locations are expected to affect the first CCR and second CCR separately. This means that if the C_{60} well depth alone is changed, it must affect only the location of first CCR; likewise, alterations in the atomic well

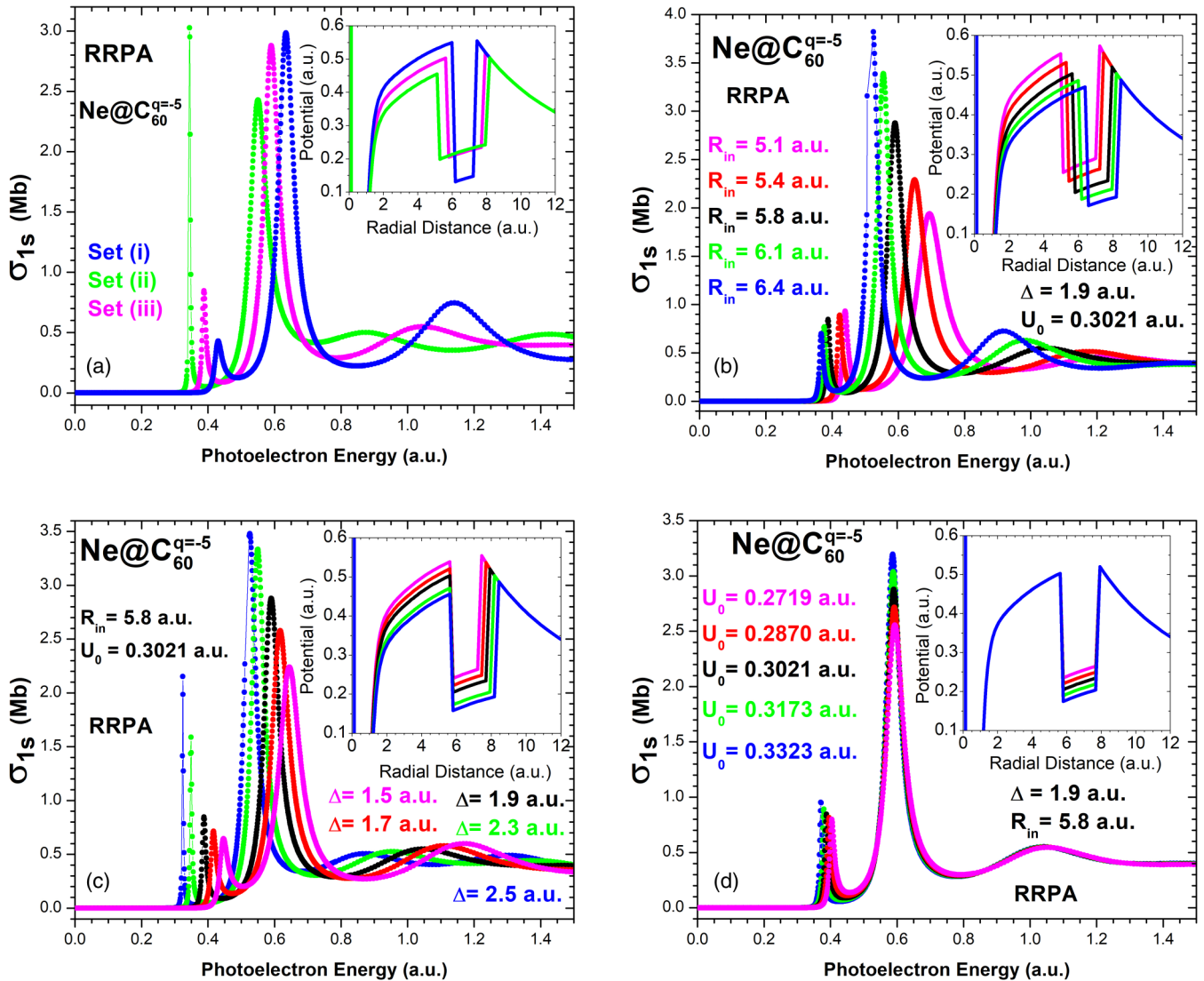


FIG. 8. (a) RRPA photoionization cross sections of Ne@C₆₀^{q=-5} using parameters listed in set (i), set (ii), and set (iii). The same employing set (iii) parameters but varying only the (b) radius (c) width and (d) depth of the potential.

will be reflected as changes in the second CCR. As the barrier height reduces, the resonances occur at lower energies which are consistently seen in Figs. 8(a)–8(c); a barrier due to the atomic well and C₆₀ well controls the second and the first CCR, respectively. It is expected because when the barrier height is reduced, the resonance condition moves to a lower energy. Parameters in Fig. 8(d) are varied in such a way that only the C₆₀ well depth is lowered. In Fig. 8(d) it is seen that the positions of the second CCR remain unaltered and this is because of the same barrier height seen by the photoelectron near the atomic well region. But, the positions of the first CCR show sensitivity to the depth of the C₆₀ potential. These findings support our prediction that the second CCR occurs due to the resonant trapping in the region of atomic well whereas the first one is due to the resonant trapping inside the confinement well. All of these are further verified by using the SAE approach (figures are not shown).

The above analysis has enabled a connection between the localization of resonant electrons and the CCR peaks in the

cross section. Nevertheless, one may find a contradiction at this point because the ground state (1s) wave function is very compact and the significant portion of its amplitude is within the first well as indicated in Fig. 6(b); it is almost zero even inside the atomic well beyond 0.5 a.u. It is well known that the main contribution to the cross section is due to the overlapping of initial and final states occurring in this region, as indicated in Eq. (5). The overlapping region for the CCRs is within a range of 0–0.5 a.u., which is far from the resonant electron localization of both CCRs. The contradiction lies in the separation of the overlapping region and the resonant electron localization region. In other words, the fact that “the localization leading to the resonant structure” is unclear due to the separation of these regions; the contradiction can be only mitigated by drawing a connection between these two regions. In order to establish the link between overlapping and localization regions, the rate of change of the maximum of the probability density distribution in these two regions is plotted. In Fig. 9(a) is shown the rate of change of the maximum

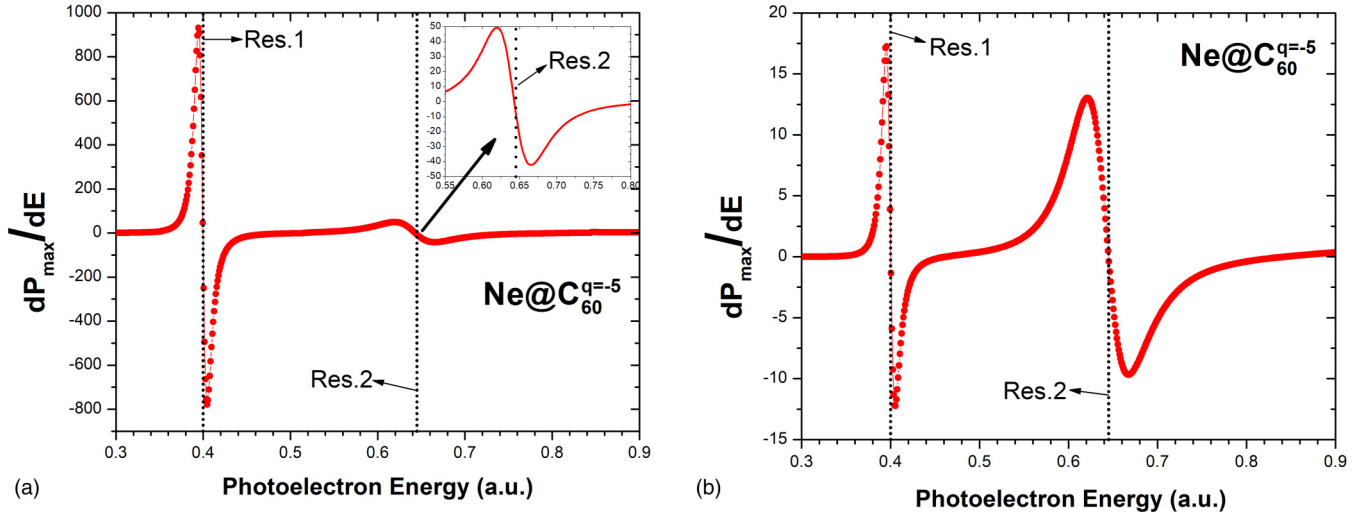


FIG. 9. (a) The rate of change of probability density maximum in the localization region. Probability density distribution maximum is taken between 1.5 and 8.5 a.u. radial distance. (b) The rate of change of probability density maximum in the atomic well (overlapping) region. Probability density distribution maximum is taken up to 1.5 a.u. radial distance. Here P_{\max} is the maximum value of the probability density corresponding to the photoelectron energy E .

of probability density with energy in the localization regions of the first and second resonances. The probability density distribution maxima are taken between the radial distances 1.5 and 8.5 a.u. because the localization of both resonances occur in this region [see Figs. 6(b) and 7(b)]. The rate of change of probability maximum for the first resonance varies rapidly compared to the second resonance. The magnitude of the energy derivative is of the order of 2, while in the case of the second resonance it is of order of 1. It indicates that the reduction in the probability amplitude in the overlapping region is much more rapid for the first resonance compared to the second resonance.

Figure 9(b) is the rate of change of the probability density distribution maxima in the overlapping region up to 1.5 a.u. radial distance where the initial $1s$ state has a significant magnitude. One may find a surprising similarity between Figs. 9(a)

and 9(b), which indicates that the characteristics of the continuum orbital in the overlapping region (contributing to the CCR) is solely inherited by those in the resonant region. For the first resonance, rate of change is very rapid and for the second resonance the variation is slow and smooth, inheriting the corresponding behavior from the localization region. It explains why the first resonance is very sharp and the second one is relatively broad. Hence the connection between the overlapping and the localization region is established, which facilitates a link between resonant localization and the CCR peaks. Since the continuum wave depends only on the photoelectron energy and the angular momentum the analysis carried out for the $1s$ subshell remains the same for the $2s$ case as well.

As seen earlier from Figs. 3 and 4, the $1s$ and $2s$ results of $\text{Ar}@C_{60}^{q=-4}$ and $\text{Xe}@C_{60}^{q=-3}$ also show a narrow resonance in the low energy region and a broad resonance at a higher energy region. Further, it is seen that the broad structure appears in the Xe $1s$ and $2s$ cross sections even for the $q = 0$ case. In order to test the conclusions drawn from $\text{Ne}@C_{60}^{q=-5}$, the SAE calculations are performed for $\text{Ar}@C_{60}^{q=-4}$ and $\text{Xe}@C_{60}^{q=-3}$. In both the cases it is found that (figures not shown) corresponding to the narrow resonance there is a localization inside the confinement well region and to the broad resonance there is a localization within the atomic well region. Lastly, we need to reassert that the resonances similar to CCRs are even supported in the $q = 0$ case, for accomplishing which the probability density of the photoelectron coming from $\text{Xe}@C_{60}$ is plotted at the peak of the observed broad resonance and is shown in Fig. 10. Here again, we see that localization associated with the broad resonance structure appears within the atomic well region, which is akin to the second CCR in the case of $\text{Ne}@C_{60}^{q=-5}$, $\text{Ar}@C_{60}^{q=-4}$, and $\text{Xe}@C_{60}^{q=-3}$. Thus the present analysis confirms that resonances similar to the CCRs are even supported by the neutral C_{60} .

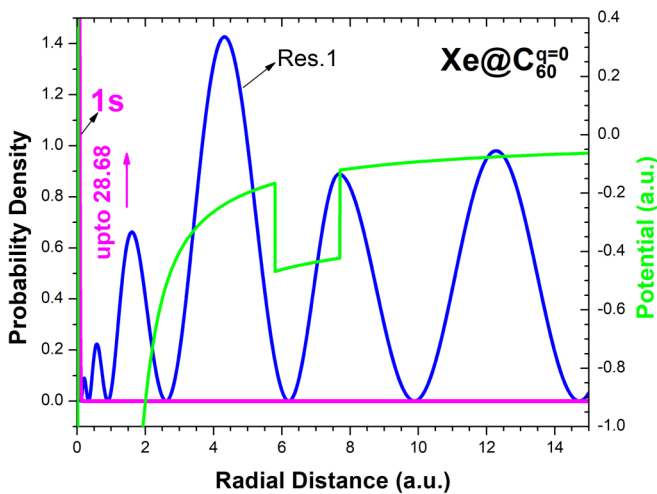


FIG. 10. Probability density of continuum state of the first resonant peak of $\text{Xe}@C_{60}^{q=0}$ along with potential seen by the photoelectron εp . Ground state probability density is also plotted.

IV. SUMMARY AND CONCLUSIONS

In this work, systematic photoionization studies of $\text{Ne}@C_{60}^q$, $\text{Ar}@C_{60}^q$, and $\text{Xe}@C_{60}^q$ have been carried out. The presence of charge induces additional structures (CCRs) in the $1s$ spectra $\text{Ar}@C_{60}^q$ and $\text{Xe}@C_{60}^q$ which are similar to the earlier predicted case of $\text{Ne}@C_{60}^q$. In addition, the present work reveals that CCRs appear in the $2s$ subshell of all these systems. It is found that although $1s$ CCRs are independent of the interchannel coupling the $2s$ CCRs are sensitive to the correlations present in the system. Moreover, the present work carried out an in-depth analysis on the origin of these CCRs and it shows that resonant trapping of the photoelectron occurs at different regions for the first and second resonances. For the broad resonance localization occurs inside the atomic well supported by the additional charges on the C_{60} whereas the narrow resonance results from the resonant trapping of the continuum wave inside the C_{60} confinement well. The

sensitivity of these resonances to different model confinement potentials is also studied. We also predict that the broad resonances can occur even for the case of neutral fullerene as shown for the case of $\text{Xe}@C_{60}^{q=0}$. It will be interesting to look into the differences in the Wigner time delay in the region of these narrow and broad resonances; the study on latter has already been reported [13]. An insightful connection can be drawn between the tunneling time and different origins of resonances from the proposed time delay analysis.

ACKNOWLEDGMENTS

H.R.V. appreciates the support from DST-SERB, India under Grant No. EMR/2016/002695 and J.J. acknowledges support from DST-SERB, India under Grant No. ECR/2016/001564.

-
- [1] W. Harneit, C. Boehme, S. Schaefer, K. Huebener, K. Fostiropoulos, and K. Lips, Room Temperature Electrical Detection of Spin Coherence in C_{60} , *Phys. Rev. Lett.* **98**, 216601 (2007).
- [2] R. H. Zadik, Y. Takabayashi, G. Klupp, R. H. Colman, A. Y. Ganin, A. Potočnik, P. Jeglič, D. Arčon, P. Matus, K. Kamarás *et al.*, Optimized unconventional superconductivity in a molecular Jahn-Teller metal, *Sci. Adv.* **1**, e1500059 (2015).
- [3] J. B. Melanko, M. E. Pearce, and A. K. Salem, Nanotubes, nanorods, nanofibers, and fullerenes for nanoscale drug delivery, in *Nanotechnology in Drug Delivery* (Springer, New York, 2009), pp.105–127.
- [4] R. B. Ross, C. M. Cardona, D. M. Guldi, S. G. Sankaranarayanan, M. O. Reese, N. Kopidakis, J. Peet, B. Walker, G. C. Bazan, E. Van Keuren, B. C. Holloway *et al.*, Endohedral fullerenes for organic photovoltaic devices, *Nat. Mater.* **8**, 208 (2009).
- [5] Y. Zhao, Y.-H. Kim, A. C. Dillon, M. J. Heben, and S. B. Zhang Hydrogen Storage in Novel Organometallic Buckyball, *Phys. Rev. Lett.* **94**, 155504 (2005).
- [6] L. Becker, R. J. Poreda, and T. E. Bunch, Fullerenes: An extraterrestrial carbon carrier phase of noble gases, *Proc. Natl. Acad. Sci. USA* **97**, 2979 (2000).
- [7] H. R. Varma, P. C. Deshmukh, V. K. Dolmatov, and S. T. Manson, Correlation and relativistic effects on the photoionization of confined atoms, *Phys. Rev. A* **76**, 012711 (2007).
- [8] T. W. Gorczyca, M. F. Hasoglu, and S. T. Manson, Photoionization of endohedral atoms using R -matrix methods: Application to $\text{Xe}@C_{60}$, *Phys. Rev. A* **86**, 033204 (2012).
- [9] P. C. Deshmukh, A. Mandal, S. Saha, A. S. Kheifets, V. K. Dolmatov, and S. T. Manson, Attosecond time delay in the photoionization of endohedral atoms $A@C_{60}$: A probe of confinement resonances, *Phys. Rev. A* **89**, 053424 (2014).
- [10] S. Saha, A. Thuppilakkadan, H. R. Varma, and J. Jose, Photoionization dynamics of endohedrally confined atomic H and Ar: A contrasting study between compact versus diffused model potential, *J. Phys. B: At. Mol. Opt. Phys.* **52**, 145001 (2019).
- [11] M. E. Madjet, H. S. Chakraborty, and S. T. Manson, Giant Enhancement in Low Energy Photoemission of Ar Confined in C_{60} , *Phys. Rev. Lett.* **99**, 243003 (2007).
- [12] J. P. Connerade, V. K. Dolmatov, P. A. Lakshmi, and S. T. Manson, Electron structure of endohedrally confined atoms: Atomic hydrogen in an attractive shell, *J. Phys. B: At. Mol. Opt. Phys.* **32**, L239 (1999).
- [13] A. Kumar, H. R. Varma, P. C. Deshmukh, S. T. Manson, V. K. Dolmatov, and A. Kheifets, Wigner photoemission time delay from endohedral anions, *Phys. Rev. A* **94**, 043401 (2016).
- [14] V. K. Dolmatov, Spin-polarized photoelectron fluxes from fullerene anions, *Atoms* **8**, 65 (2020).
- [15] V. K. Dolmatov, A. S. Baltenkov, J.-P. Connerade, and S. T. Manson, Structure and photoionization of confined atoms, *Radiat. Phys. Chem.* **70**, 417 (2004).
- [16] V. K. Dolmatov, *Photoionization of Atoms Encaged in Spherical Fullerenes, Advances in Quantum Chemistry* (Academic Press, New York, 2009), Vol. 58, pp.13–68.
- [17] V. K. Dolmatov, P. Brewer, and S. T. Manson, Photoionization of atoms confined in giant single-walled and multiwalled fullerenes, *Phys. Rev. A* **78**, 013415 (2008).
- [18] H. S. Chakraborty, M. E. Madjet, T. Renger, J.-M. Rost, and S. T. Manson, Photoionization of hybrid states in endohedral fullerenes, *Phys. Rev. A* **79**, 061201 (2009).
- [19] A. Mandal, P. C. Deshmukh, A. S. Kheifets, V. K. Dolmatov, and S. T. Manson, Angle-resolved wigner time delay in atomic photoionization: the 4d subshell of free and confined Xe, *Phys. Rev. A* **96**, 053407 (2017).
- [20] A. S. Baltenkov, Resonances in photoionization cross sections of inner subshells of atoms inside the fullerene cage, *J. Phys. B: At. Mol. Opt. Phys.* **32**, 2745 (1999).
- [21] A. B. Patel and H. S. Chakraborty, Fourier photospectroscopy of $\text{Xe}@C_{60}$ through a Xe 4d resonance window: theory versus recent experiment, *J. Phys. B: At. Mol. Opt. Phys.* **44**, 191001 (2011).
- [22] K. Govil and P. C. Deshmukh, Quadrupole photoionization of endohedral $\text{Xe}@C_{60}$, *J. Phys. B: At. Mol. Opt. Phys.* **42**, 175003 (2009).

- [23] K. Govil, A. J. Siji, and P. C. Deshmukh, Relativistic and confinement effects in photoionization of Xe, *J. Phys. B: At. Mol. Opt. Phys.* **42**, 65004 (2009).
- [24] D. A. Keating, P. C. Deshmukh, and S. T. Manson, Wigner time delay and spin-orbit activated confinement resonances, *J. Phys. B: At. Mol. Opt. Phys.* **50**, 175001 (2017).
- [25] V. K. Dolmatov, M. B. Cooper, and M. E. Hunter, Electron elastic scattering off endohedral fullerenes A@C₆₀: The initial insight, *J. Phys. B: At. Mol. Opt. Phys.* **47**, 115002 (2014).
- [26] V. K. Dolmatov, C. Bayens, M. B. Cooper, and M. E. Hunter, Electron elastic scattering and low-frequency bremsstrahlung on A@C₆₀: A model static-exchange approximation, *Phys. Rev. A* **91**, 062703 (2015).
- [27] A. Müller, S. Schippers, M. Habibi, D. Esteves, J. C. Wang, R. A. Phaneuf, A. L. D. Kilcoyne, A. Aguilar, and L. Dunsch, Significant Redistribution of Ce 4d Oscillator Strength Observed in Photoionization of Endohedral Ce@C₈₂⁺ Ions, *Phys. Rev. Lett.* **101**, 133001 (2008).
- [28] R. A. Phaneuf, A. L. D. Kilcoyne, N. B. Aryal, K. K. Baral, D. A. Esteves-Macaluso, C. M. Thomas, J. Hellhund, R. Lomsadze, T. W. Gorczyca, C. P. Ballance *et al.*, Probing confinement resonances by photoionizing Xe inside a C₆₀⁺ molecular cage, *Phys. Rev. A* **88**, 053402 (2013).
- [29] A. L. D. Kilcoyne, A. Aguilar, A. Müller, S. Schippers, C. Cisneros, G. Alna'Washi, N. B. Aryal, K. K. Baral, D. A. Esteves, C. M. Thomas *et al.*, Confinement Resonances in Photoionization of Xe@C₆₀⁺, *Phys. Rev. Lett.* **105**, 213001 (2010).
- [30] V. K. Dolmatov and S. T. Manson, Photoionization of atoms encapsulated in endohedral ions A@C₆₀^{±z}, *Phys. Rev. A* **73**, 013201 (2006).
- [31] A. Thuppilakkadan and H. R. Varma, Photoresponse studies of Ar and K⁺ confined in neutral and charged Fullerenes, *J. Phys. Conf. Ser.* **1412**, 102006 (2020).
- [32] V. K. Dolmatov, G. T. Craven, E. Guler, and D. Keating, Revivification of confinement resonances in the photoionization of A@C₆₀ endohedral atoms far above thresholds, *Phys. Rev. A* **80**, 035401 (2009).
- [33] X. M. Tong and C. D. Lin, Empirical formula for static field ionization rates of atoms and molecules by lasers in the barrier-suppression regime, *J. Phys. B: At. Mol. Opt. Phys.* **38**, 2593 (2005).
- [34] J. George, H. R. Varma, P. C. Deshmukh, and S. T. Manson, Photoionization of atomic krypton confined in the fullerene C₆₀, *J. Phys. B: At. Mol. Opt. Phys.* **45**, 185001 (2012).
- [35] W. R. Johnson and K. T. Cheng, Photoionization of the outer shells of neon, argon, krypton, and xenon using the relativistic random-phase approximation, *Phys. Rev. A* **20**, 978 (1979).
- [36] W. R. Johnson and K. T. Cheng, Relativistic Effects on Low-Energy 5s → εp Photoionization for Xenon, *Phys. Rev. Lett.* **40**, 1167 (1978).
- [37] W. R. Johnson and C. D. Lin, Multichannel relativistic random-phase approximation for the photoionization of atoms, *Phys. Rev. A* **20**, 964 (1979).
- [38] M.-H. Yuan and X.-B. Bian, Angular distribution of photoelectron momentum in above-threshold ionization by circularly polarized laser pulses, *Phys. Rev. A* **101**, 013412 (2020).
- [39] M. Kunitski, N. Eicke, P. Huber, J. Köhler, S. Zeller, J. Voigtsberger, N. Schlott, K. Henrichs, H. Sann, F. Trinter *et al.*, Double-slit photoelectron interference in strong-field ionization of the neon dimer, *Nat. Commun.* **10**, 1 (2019).
- [40] M. Kübel, G. P. Katsoulis, Z. Dube, A. Y. Naumov, D. M. Villeneuve, P. B. Corkum, A. Staudte, and A. Emmanouilidou, Streaking strong-field double ionization, *Phys. Rev. A* **100**, 043410 (2019).
- [41] Q. Zhang, P. Lan, and P. Lu, Empirical formula for over-barrier strong-field ionization, *Phys. Rev. A* **90**, 043410 (2014).
- [42] L. Ley and M. Cardona, in *Photoemission in Solids II: Case Studies* (Springer, Berlin, 1979), Vol. 27, Appendix, pp.373–384.
- [43] J. A. Bearden and A. F. Burr, Reevaluation of x-ray atomic energy levels, *Rev. Mod. Phys.* **39**, 125 (1967).
- [44] B. H. Bransden and C. J. Joachain, *Physics of Atoms and Molecules* (Pearson Education, New Delhi, 2003).
- [45] S. Saha, A. Mandal, J. Jose, H. R. Varma, P. C. Deshmukh, A. S. Kheifets, V. K. Dolmatov, and S. T. Manson, Relativistic effects in photoionization time delay near the cooper minimum of noble-gas atoms, *Phys. Rev. A* **90**, 053406 (2014).
- [46] M. Y. Amusia, The random-phase approximation with exchange, in *Atomic Photoeffect* (Springer, Boston, 1990), pp.99–145.
- [47] E. W. B. Dias, H. S. Chakraborty, P. C. Deshmukh, S. T. Manson, O. Hemmers, P. Glans, D. L. Hansen, H. Wang, S. B. Whitfield, D. W. Lindle *et al.*, Breakdown of the Independent Particle Approximation in High-Energy Photoionization, *Phys. Rev. Lett.* **78**, 4553 (1997).
- [48] J. Jose, G. B. Pradhan, V. Radojević, S. T. Manson, and P. C. Deshmukh, Electron correlation effects near the photoionization threshold: the Ar isoelectronic sequence, *J. Phys. B: At. Mol. Opt. Phys.* **44**, 195008 (2011).
- [49] C. Winstead and V. McKoy, Elastic electron scattering by fullerene, C₆₀, *Phys. Rev. A* **73**, 012711 (2006).
- [50] V. K. Dolmatov and D. A. Keating, Xe 4d photoionization in Xe@C₆₀, Xe@C₂₄₀, and Xe@C₆₀@C₂₄₀, *J. Phys. Conf. Ser.* **388**, 022097 (2012).